Research article

Stephen Sanders and Alejandro Manjavacas*

Nanoantennas with balanced gain and loss

https://doi.org/10.1515/nanoph-2019-0392
Received September 28, 2019; revised November 21, 2019; accepted December 2, 2019

Abstract: The large cross sections and strong confinement provided by the plasmon resonances of metallic nanostructures make these systems an ideal platform to implement nanoantennas. Like their macroscopic counterparts, nanoantennas enhance the coupling between deep subwavelength emitters and free radiation, providing, at the same time, an increased directionality. Here, inspired by the recent works in parity-time symmetric plasmonics, we investigate how the combination of conventional plasmonic nanostructures with active materials, which display optical gain when externally pumped, can serve to enhance the performance of metallic nanoantennas. We find that the presence of gain, in addition to mitigating the losses and therefore increasing the power radiated or absorbed by an emitter, introduces a phase difference between the elements of the nanoantenna that makes the optical response of the system directional, even in the absence of geometrical asymmetry. Exploiting these properties, we analyse how a pair of nanoantennas with balanced gain and loss can enhance the far-field interaction between two dipole emitters. The results of this work provide valuable insight into the optical response of nanoantennas made of active and passive plasmonic nanostructures, with potential applications for the design of optical devices capable of actively controlling light at the nanoscale.

Keywords: nanoantenna; PT symmetry; gain; active materials; asymmetric response.

1 Introduction

The coherent oscillation of the conduction electrons of metallic nanostructures, commonly known as surface plasmons, is capable of strongly interacting with light and confining it into volumes with subwavelength dimensions [1]. Thanks to these extraordinary properties, metallic nanostructures have become an ideal platform to implement nanoantennas, the nanoscale counterpart of macroscopic antennas [2, 3]. These devices serve to maximise the transfer of energy between free radiation and subwavelength emitters, such as atoms, molecules, or quantum dots, and to provide, simultaneously, an increased directionality to the radiation-emitter coupling [4–6]. For these reasons, nanoantennas are being exploited for a variety of applications, including photodetection [7–9], light emission [10, 11], photovoltaics [12, 13], sensing [14–17], and spectroscopy [18, 19].

Metallic nanoantennas can benefit from the incorporation of active materials displaying optical gain, which, in addition to reducing the material losses inherent to metals [20–22], can be exploited to achieve strongly asymmetric optical responses [23]. Indeed, nanostructures composed of elements with balanced gain and loss are the subject of extensive research as platforms to implement parity-time (PT) symmetric plasmonic systems [24, 25]. Thanks to the interplay between gain and loss, these systems display extraordinary properties, such as unidirectional cloaking [26], switching [27], routing [28], and multiplexing [29], nonreciprocal responses [30–35], transition from absorption to amplification in cavities [36] and waveguides [37, 38], anisotropic emission [39, 40] and scattering [41–45], anomalous optical forces [46, 47], improved sensing capabilities [48], polarisation control [49], and giant near-field radiative heat transfer [50].

In this context, we have recently shown that a dimer composed of two identical plasmonic nanospheres, one with an active response and the other with a passive behaviour, displays asymmetric scattering and absorption cross sections, despite its perfectly symmetrical geometry [41]. Here, inspired by this result, we investigate how the combination of plasmonic nanostructures with balanced gain and loss enables the implementation of directional nanoantennas with tunable responses. Specifically, we find that the presence of gain serves simultaneously to enhance the emission and absorption of radiation by an emitter placed at the centre of the dimer and to introduce a phase difference between the elements of the

***Corresponding author: Alejandro Manjavacas,** Department of Physics and Astronomy, University of New Mexico, Albuquerque, NM 87131, USA, e-mail: manjavacas@unm.edu. https://orcid.org/0000-0002-2379-1242
Stephen Sanders: Department of Physics and Astronomy, University of New Mexico, Albuquerque, NM 87131, USA. https://orcid.org/0000-0001-6001-9828

nanoantenna that provides directionality to the emission and absorption of the emitter. Using these results, we analyse how nanoantennas with balanced gain and loss can mediate the transfer of energy between pairs of emitters separated by a distance much larger than their resonant wavelengths. Our results show that the presence of active materials can be used as a mechanism to actively control the relative phase between plasmonic nanostructures, thus enabling the design of actively tunable nanoantennas with directional responses.

2 Results and analysis

The system under study consists of a dimer composed of two spherical nanoparticles of radius $R=100$ nm separated by a centre-to-centre distance $d=250$ nm, as shown in Figure 1A. One of the particles (blue) has a passive metallic response that we describe using the Drude dielectric function [1]

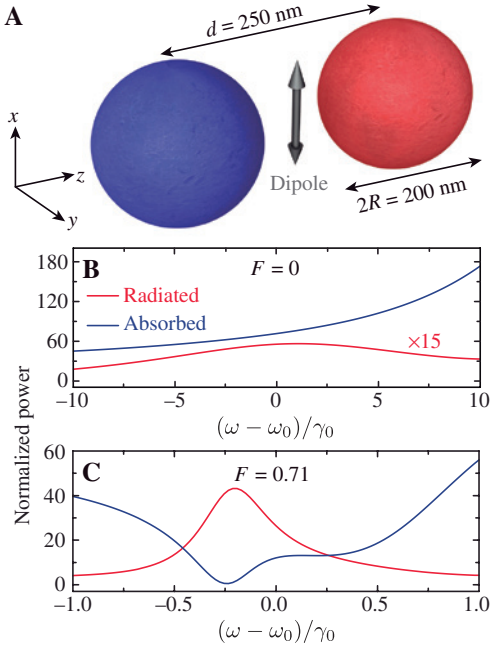

Figure 1: Analysis of the absorbed and radiated power. (A) Schematics of the system under study, consisting of two spherical nanoparticles with a radius $R=100$ nm separated by a centre-to-centre distance $d=250$ nm, which are excited by a dipole source placed in the centre of their gap. One particle has a conventional passive plasmonic response (blue), whereas the other displays optical gain (red). (B, C) Total power radiated (red curve) and absorbed (blue curve) by the dimer when excited by the dipole. These quantities are normalised to the power radiated by a dipole $\mathbf{p}_0$ in vacuum $P_0=4\omega^4|\mathbf{p}_0|^2/(3c^3)$. In B, we assume a fully passive dimer (i.e. $F=0$), whereas in C, the pumping parameter is set to $F=0.71$. Notice that in B the red curve is multiplied by 15 to improve visibility.

$$\varepsilon_L(\omega)=\varepsilon_\infty-\frac{\omega_p^2}{\omega(\omega+i\gamma_p)},$$

with $\varepsilon_\infty=2$, $\hbar\omega_p=2$ eV, and $\gamma_p=0.05\omega_p$, which are realistic values for transparent conductive oxides at frequencies below their band gap [51]. The other particle (red) is made from the same metallic material but has an active response arising from being doped with a gain material, which we model by adding a Lorentzian gain term to the dielectric function,

$$\varepsilon_G(\omega)=\varepsilon_L(\omega)+F\frac{\gamma_0}{\omega-\omega_0+i\gamma_0}.$$

This Lorentzian gain term represents the optical gain provided by optically pumped quantum emitters, such as dye molecules or rare earth ions [39, 41, 50]. This approach is justified for systems in which quantum effects are not expected to be relevant [52] and provides a good approximation to the steady-state solution of a time-dependent semiclassical description of a gain medium [53, 54]. Here, we assume $\hbar\omega_0=0.94$ eV for the gain frequency and $\gamma_0=0.01\omega_0$ for the gain bandwidth, while F, which describes the population inversion of the gain material, is left as the parameter that controls the level of gain in the system and is determined by the level of external pumping. These values are compatible with experimental measurements (see [39, 50, 55]) and references therein).

We begin our study by analysing the response of a fully passive dimer, i.e. with no external pumping, $F=0$. We calculate the total power radiated and absorbed by the dimer when excited by a dipole placed at the centre of the gap between the two nanoparticles, as shown in Figure 1A. We neglect any possible back-action of the dipole source on the material response of the particles. The corresponding results, obtained from the rigorous solution of Maxwell's equations using a finite element method, are shown in Figure 1B. We assume that the exciting dipole, which oscillates at frequency ω, is oriented perpendicular to the axis of the dimer and normalise the results to the power radiated by a dipole of amplitude $\mathbf{p}_0$ in vacuum $P_0=4\omega^4|\mathbf{p}_0|^2/(3c^3)$. Examining the results, we observe that, for $F=0$, the power absorbed by the dimer (blue curve) is more than 15 times larger than the radiated power (red curve, notice the scaling factor), and therefore the system behaves as a poor nanoantenna. However, this behaviour is dramatically changed when the pumping parameter is set to $F=0.71$, a value chosen to ensure that the absorption of the system still remains positive, and therefore the

system does not reach a lasing threshold. In this case, as shown in Figure 1C, the radiated power increases, and simultaneously, the absorbed power is reduced, almost vanishing near ω_0. This results in a frequency range around ω_0 in which the radiated power dominates over the absorbed power, and hence, the dimer acts as an efficient nanoantenna. Interestingly, both the radiated power and absorbed power display a monotonic behaviour with the increase in the gain, as shown in Figure 2. Furthermore, it is worth noting that the normalised radiated and absorbed power shown in Figures 1 and 2 are, respectively, equal to the radiative and nonradiative components of the local density of optical states (LDOS) when normalised to the LDOS of vacuum.

The increase in F, in addition to mitigating the absorption losses of the system and therefore enhancing the power radiated, also serves to introduce a phase difference in the optical response of the nanoparticles. This phase difference, which ultimately arises from the negative imaginary part of the dielectric function of the gain material, can be exploited to achieve directionality in the radiated power [56]. From the perspective of PT symmetric systems, the increase in the gain brings the system closer to the point in which the gain compensates the losses and therefore is expected to produce an asymmetric response [30, 57, 58]. To analyse this possibility, in Figure 3A, we calculate the power radiated by the dimer along its axis, both in the direction of the gain side ($\theta = 0°$) and in the direction of the loss side ($\theta = 180°$), as depicted in the inset. The corresponding results, normalised to P_0, are plotted using red and blue curves, respectively. We perform this calculation for increasing values of the pumping parameter F below $F = 0.71$, for which, as discussed before, the absorbed power remains positive, thus ensuring we are far from any lasing threshold, and for a frequency detuning $\omega - \omega_0 = -0.19\gamma_0$. As expected, for $F = 0$, the radiated power is completely symmetric; however, as this parameter grows, the power radiated becomes increasingly asymmetric. This is illustrated by the black dashed curve, which represents the ratio between the power radiated along the two directions. Clearly, this quantity grows monotonically from 1, for the completely passive dimer (i.e. $F = 0$), to almost 3 when the pumping parameter is increased to $F = 0.71$. The lack of a

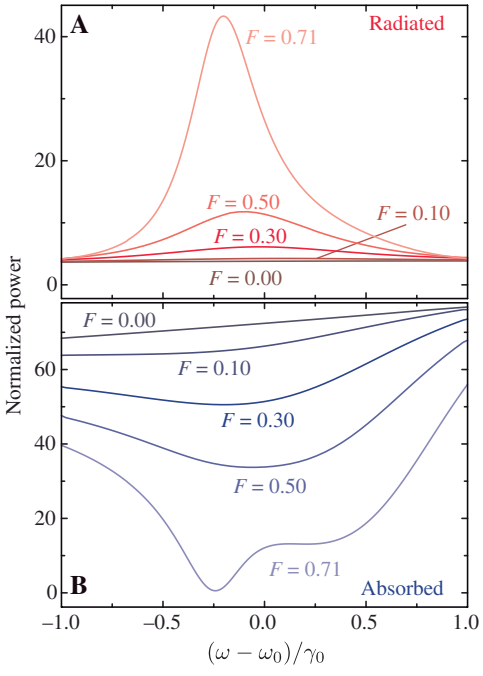

Figure 2: Detailed analysis of the absorbed and radiated power. Total power radiated (A) and absorbed (B) by the active–passive dimer when excited by a dipole source, calculated for increasing values of F. Both quantities are normalised to P_0.

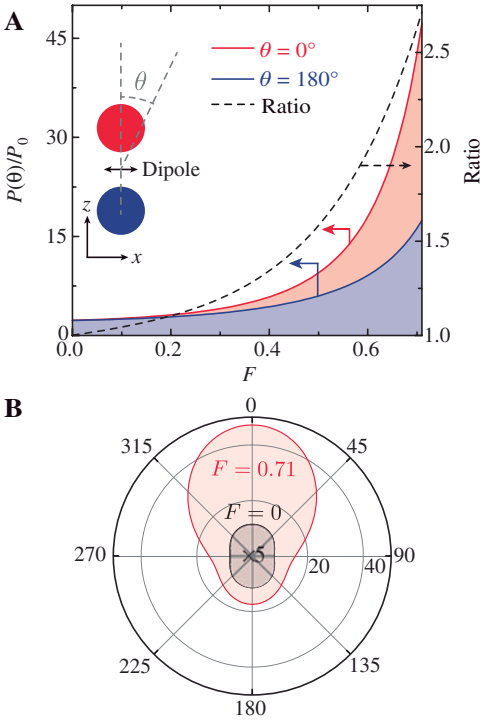

Figure 3: Analysis of the directionality of the power radiated. (A) Power radiated by the dimer along its axis in the direction of the gain side, $\theta = 0°$ (red solid curve), and the loss side, $\theta = 180°$ (blue solid curve), normalised to P_0 (left axis). This quantity is plotted as a function of the pumping parameter F for a detuning $\omega - \omega_0 = -0.19\gamma_0$. The black dashed curve (right axis) shows the ratio between the power radiated along the two aforementioned directions. (B) Angular distribution of the power radiated by the system for $F = 0.71$ (red curve) compared with that of the passive dimer, $F = 0$ (black curve). Note that the latter is multiplied by 5 to improve the visibility.

threshold behaviour indicates that the asymmetry does not directly result from an exceptional point [59]. For $F = 0.71$, the power radiated by the dimer displays a strong imbalance toward the direction of the gain particle, as can be seen from the analysis of the full angular distribution plotted in Figure 3B. In this plot, the red curve represents the angular distribution of the power radiated by the active–passive dimer with $F = 0.71$, whereas the black curve represents the results for the completely passive dimer ($F = 0$). Therefore, the presence of gain, in addition to increasing the power radiated by more than one order of magnitude as compared with the passive dimer (note the scaling factor), directs the energy predominantly toward the gain side of the dimer.

We can gain a deeper insight into the optical response of the active–passive dimer by using a simple dipolar approach, in which each of the nanoparticles is modelled as a point dipole. Within this approximation, the optical response of the passive and active particles is described using the frequency-dependent polarisabilities α_L and α_G, respectively. We assume that these polarisabilities already incorporate the corrections arising from the mutual interaction between the nanoparticles. Then, as shown in Appendix B, the power radiated at an angle θ by the dimer and the dipole emitter can be written as

$$\frac{P(\theta)}{P_0} = \frac{3}{8}(1+\cos^2\theta)\Big[1+|G_0\alpha_G|^2+|G_0\alpha_L|^2 +2|G_0|^2\,\mathrm{Re}\left\{e^{-ikd\cos\theta}\alpha_G\alpha_L^* + e^{-ik\frac{d}{2}\cos\theta}\left(\frac{\alpha_G}{G_0^*}+\frac{\alpha_L^*}{G_0}\right)\right\}\Big], \tag{1}$$

where $G_0 = e^{ikd/2}[2k^2/d + 4ik/d^2 - 8/d^3]$ is the dipole–dipole interaction tensor connecting the dipole source with the dipoles induced in either of the two particles. Using this expression, we can write the ratio of the power radiated along the $\theta = 0°$ and $\theta = 180°$ directions as $(1+\beta)/(1-\beta)$ with

$$\beta = \frac{2|G_0|^2\sin(kd)\mathrm{Im}\{\alpha_G\alpha_L^*\} + 2\sin(kd/2)\mathrm{Im}\{G_0(\alpha_G-\alpha_L)\}}{1+|G_0|^2(|\alpha_G|^2+|\alpha_L|^2+2\cos(kd)\mathrm{Re}\{\alpha_G\alpha_L^*\}) + 2\cos(kd/2)\mathrm{Re}\{G_0(\alpha_G+\alpha_L)\}}.$$

This expression confirms that, for a completely passive system (i.e. $F = 0$), in which the two particles are identical ($\alpha_G = \alpha_L$), $\beta = 0$, and hence, there is no asymmetry in the radiated power. It also shows that it is possible to achieve an asymmetric radiation pattern by introducing a phase difference in the response of the two elements of the dimer, such that the numerator of this expression does not vanish. One way of achieving this is by using nanostructures with different geometries [56], as is the case for the Yagi–Uda nanoantenna [4]. Another option is what we discuss in this work, that is, the combination of nanostructures with balanced gain and loss. Specifically, as F increases, the dimer approaches the point for which $\alpha_G = \alpha_L^*$, thus making $\beta \neq 0$, in complete agreement with the asymmetric radiation pattern analysed in Figure 3. Incidentally, this mechanism has the added feature that it can be actively controlled through the tuning of the external pumping, thus enabling the possibility of adjusting the level of asymmetry in the radiated power.

So far, we have analysed the behaviour of the active–passive dimer under a dipole excitation and shown that the system is capable of acting as a tunable antenna in transmitter mode, that is, enhancing and directing the power radiated by the dipole along the axis of the dimer in the direction of the gain particle. However, in order to complete the characterisation of this system, we need to analyse its performance when acting in receiver mode. To that end, in Figure 4, we study the field intensity enhancement, FE(θ), produced by the dimer at the centre of its gap when it is illuminated with a plane wave. We define this quantity as the ratio between the squared magnitude of the x component of the electric field at the centre of the gap and that of the incident plane wave. Furthermore, we assume that the plane wave propagates toward the dimer at an angle θ and is polarised parallel to the plane of incidence (i.e. in the xz plane), as shown in the inset. The red and blue curves show the results for the active–passive dimer, with $F = 0.71$, when illuminated at $\theta = 0°$ and $\theta = 180°$, respectively. Analysing these results, we conclude that the field intensity at the gap displays a strongly asymmetrical behaviour, being almost 3 times larger when the plane wave impinges from the gain side of the dimer. This asymmetric behaviour is in sharp contrast with the results obtained for the completely passive dimer (black curve), which are identical for the two different illumination angles. Furthermore, as was the case for a dipole excitation, the presence of gain also enhances the response of the system through the mitigation of its losses, thus resulting in a field intensity that is 21 times larger than that produced by the completely passive dimer. It is worth noting that this asymmetric response could have been obtained from the results of Figure 3 by exploiting Lorentz reciprocity [60] (Appendix C).

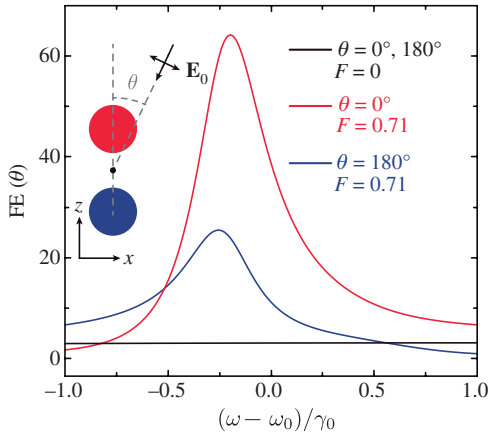

Figure 4: Analysis of the directionality of the field intensity enhancement.
Field intensity enhancement, FE(θ), at the centre of the dimer gap when the system is illuminated with a plane wave. As shown in the inset, we assume the plane wave to propagate toward the dimer at an angle θ and to be polarised parallel to the xz plane. The colour curves display the results for an active–passive dimer with $F=0.71$ when $\theta=0°$ (red curve) and $\theta=180°$ (blue curve), whereas the black curve indicates the results for a completely passive dimer (i.e. $F=0$). Notice that, in this case, the results for $\theta=0°$ and $\theta=180°$ are identical.

Based on the results of Figures 3 and 4, we anticipate that a pair of active–passive dimers can efficiently mediate the transfer of energy between two emitters separated by a distance much larger than their resonant wavelengths, i.e. in the far-field region. In particular, consider the pair of nanoantennas depicted in the upper panel of Figure 5A, and assume that the dipole in the leftmost dimer acts as the emitter, whereas the one in the rightmost dimer serves as the receiver. Thanks to the combination of (i) the enhancement of the radiated power and (ii) the increased field at the gap of the dimer, which we analysed, respectively, in Figures 3 and 4, we expect the energy transfer between the two dipoles to be greatly enhanced in this arrangement, which we denote as the LGGL configuration. On the contrary, when the orientation of the dimers is reversed, as in the GLLG configuration shown in the lower panel of Figure 5A, we expect a much smaller energy transfer. In order to verify this hypothesis, we compute the normalised energy transfer rate (nETR) [61, 62], defined as

$$\mathrm{nETR}=\frac{|\hat{\mathbf{n}}_r\cdot\mathbf{E}_e(\mathbf{r}_r)|^2}{|\hat{\mathbf{n}}_r\cdot\mathbf{E}_{e,0}(\mathbf{r}_r)|^2}.$$

Here, $\hat{\mathbf{n}}_r$ is a unit vector oriented as the receiver dipole, $\mathbf{E}_e(\mathbf{r}_r)$ is the electric field produced by the emitter dipole at the position of the receiver when each dipole is placed in the gap of an active–passive dimer, and $\mathbf{E}_{e,0}(\mathbf{r}_r)$ is the same quantity when the dipoles are in vacuum. Assuming that the two dimers are in the far-field region of each other, we can write the following approximate expression for the nETR (Appendix C):

$$\mathrm{nETR}\approx\frac{4}{3}\frac{P(\theta)}{P_0}\mathrm{FE}(\theta), \tag{2}$$

where θ is equal either to 0° for the LGGL configuration or to 180° for the GLLG one. Figure 5B shows the results of the nETR, calculated using this expression, as a function of the pumping parameter F for a detuning $\omega-\omega_0=-0.19\gamma_0$. Red and blue curves correspond, respectively, to the LGGL and GLLG configurations. As expected, for $F=0$, both configurations result in the same nETR of approximately 10. As F grows, the nETR increases significantly with the LGGL arrangement, reaching values of several thousand when $F=0.71$. Simultaneously, the ratio between the two configurations, which is shown by the black dashed curve (right axis), grows and becomes almost 8 when $F=0.71$. These results confirm that the active–passive dimers can operate as efficient nanoantennas, which can be externally controlled through the adjustment of the pumping level.

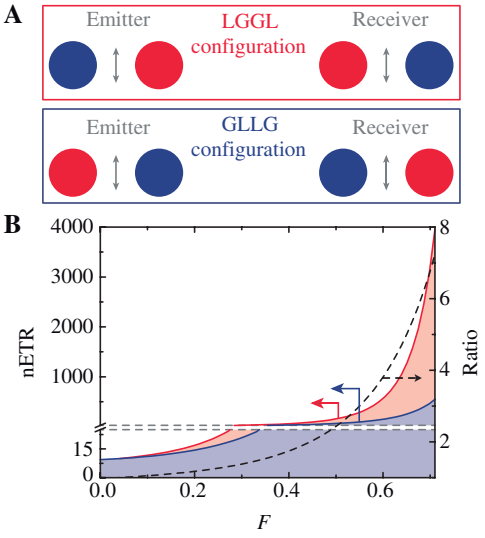

Figure 5: Analysis of the energy transfer.
(A) Schematic of a nanoantenna pair mediating the radiative transfer of energy between two emitters placed at distances much larger than their resonant wavelengths. We consider two different arrangements that we denote as LGGL and GLLG configurations, where L and G represent a passive and active nanoparticle, respectively. (B) Normalised energy transfer rate (nETR) between the two dipole emitters for the LGGL configuration (red solid curve) and the GLLG configuration (blue solid curve). This quantity is plotted as a function of the pumping parameter F for a detuning $\omega-\omega_0=-0.19\gamma_0$. Notice the axis break introduced to improve visibility for small values of F. The black dashed curve (right axis) indicates the ratio between the nETR of the LGGL and GLLG configurations.

3 Conclusion and outlook

In summary, we have investigated the optical response of a nanoparticle dimer composed of two metallic nanospheres, one with a conventional passive response and the other made from an active material, which displays optical gain when externally pumped. We have found that this system, thanks to the interplay between the gain and loss, is capable of enhancing and directing the power radiated by a dipole emitter placed at the centre of its gap. For the same reasons, when excited by a plane wave, the active–passive dimer produces a field enhancement at the centre of its gap that is strongly dependent on the direction of incidence of the plane wave. Owing to these properties, which can be explained as the result of a phase difference between the elements of the dimer introduced by the gain, the active–passive dimer can act as a directional nanoantenna, both in transmitter and receiver modes. In order to illustrate this possibility, we have analysed the nETR between two dipole emitters placed at the centre of two active–passive dimers. The results of this work show that the combination of nanostructures with balanced gain and loss provides an alternative path to achieve directional optical responses, which can complement and enhance other strategies based on tailoring the geometrical properties of the system. Furthermore, the presence of active elements provides the additional features of being tunable through the control of the external pumping and enhancing the overall optical response due to the decrease in the inherent material losses of the system.

Acknowledgements: This work has been sponsored by the US National Science Foundation (Grant ECCS-1710697). We would like to thank the UNM Center for Advanced Research Computing, supported in part by the National Science Foundation, for providing the high-performance computing resources used in this work. This article is dedicated to the memory of Dr. Alejandro Sarrion-Perdigones.

Appendix

A. Evolution of the power radiated and absorbed with the level of gain

Figure 2 shows the evolution with the level of gain of the total power radiated (A) and absorbed (B) by the active–passive dimer when excited by a dipole source. Clearly, as F increases, both the radiated power and the absorbed power display a monotonic behaviour.

B. Dipole model

Within the dipolar approximation, we can model the optical response of the active–passive dimer excited by a dipole emitter at its gap as a collection of three point dipole emitters. By doing so, the differential power radiated by the system per unit of solid angle in the direction of $\hat{\mathbf{n}}$ can be written (using Gaussian units), as

$$\frac{dP}{d\Omega}=\frac{\omega^4}{2\pi c^3}\sum_{i,j=0,G,L} e^{i\mathbf{k}\cdot(\mathbf{r}_j-\mathbf{r}_i)}[\mathbf{p}_i\cdot\mathbf{p}_j^*-(\mathbf{p}_i\cdot\hat{\mathbf{n}})(\mathbf{p}_j^*\cdot\hat{\mathbf{n}})],$$

where $\mathbf{k}=\omega/c\,\hat{\mathbf{n}}$ is the wavevector of the radiation, and $\mathbf{r}_i$ is the position of dipole i. Furthermore, $\mathbf{p}_0$ is the dipole moment of the dipole emitter, whereas $\mathbf{p}_G=\alpha_G G_0\mathbf{p}_0$ and $\mathbf{p}_L=\alpha_L G_0\mathbf{p}_0$ are the dipole moment induced in the active and passive particles, respectively. We write the latter in terms of frequency-dependent polarisabilities α_G and α_L, which we assume to already include the effect of the interaction between the two particles, and G_0, which is the dipole–dipole interaction tensor that describes the field produced by $\mathbf{p}_0$ at the position of the particles. Using the geometry shown in Figure 1A, we can rewrite this expression as

$$\begin{aligned}\frac{dP}{d\Omega}=&\frac{\omega^4}{2\pi c^3}\sum_{i=0,G,L}(|\mathbf{p}_i|^2-|\hat{\mathbf{n}}\cdot\mathbf{p}_i|^2)\\&+\frac{\omega^4}{\pi c^3}Re\{e^{-ikd\cos\theta}[\mathbf{p}_G\cdot\mathbf{p}_L^*-(\mathbf{p}_G\cdot\hat{\mathbf{n}})(\mathbf{p}_L^*\cdot\hat{\mathbf{n}})]\}\\&+\frac{\omega^4}{\pi c^3}Re\left\{e^{ik\frac{d}{2}\cos\theta}[\mathbf{p}_0\cdot\mathbf{p}_G^*-(\mathbf{p}_0\cdot\hat{\mathbf{n}})(\mathbf{p}_G^*\cdot\hat{\mathbf{n}})]\right\}\\&+\frac{\omega^4}{\pi c^3}Re\left\{e^{-ik\frac{d}{2}\cos\theta}[\mathbf{p}_0\cdot\mathbf{p}_L^*-(\mathbf{p}_0\cdot\hat{\mathbf{n}})(\mathbf{p}_L^*\cdot\hat{\mathbf{n}})]\right\},\end{aligned}$$

where d is the distance separating the gain and loss particles, and θ is the angle between the dimer axis and the unit vector $\hat{\mathbf{n}}$. After integrating this expression over the azimuthal angle and normalising to the power radiated by the $\mathbf{p}_0$ dipole in vacuum, $P_0=4\omega^4|\mathbf{p}_0|^2/(3c^3)$, we obtain (1).

C. Normalised energy transfer rate

Following previous works [61, 62], we define the normalised energy transfer rate (nETR) between two emitters placed at the gaps of a pair of active–passive dimers as

$$\text{nETR}=\frac{|\hat{\mathbf{n}}_r\cdot\mathbf{E}_e(\mathbf{r}_r)|^2}{|\hat{\mathbf{n}}_r\cdot\mathbf{E}_{e,0}(\mathbf{r}_r)|^2},\qquad(3)$$

where $\hat{\mathbf{n}}_r$ corresponds to the unit vector parallel to the receiver dipole, whereas $\mathbf{E}_e(\mathbf{r}_r)$ and $\mathbf{E}_{e,0}(\mathbf{r}_r)$ represent the electric field produced by the emitter dipole at the position

of the receiver in presence of the active–passive dimers and in vacuum, respectively.

Assuming that the two dimers are located in the far-field region of each other, the field radiated by the emitter dipole can be written as a spherical wave [63] $\mathbf{f}e^{ikr}/r$, with r being the distance between the emitter and the receiver dipoles, and $\mathbf{f}$, the far-field amplitude. This spherical wave can be approximated, at the position of the receiver dimer, as a plane wave, and therefore, we can write (3) as

$$\mathrm{nETR} \approx \frac{|\mathbf{f}|^2}{|\mathbf{f}_0|^2}\mathrm{FE}(\theta),$$

where $\mathrm{FE}(\theta)$ is the field intensity enhancement (Figure 4), and $\mathbf{f}_0 = k^2[\mathbf{p}_e - \hat{\mathbf{n}}(\hat{\mathbf{n}}\cdot\mathbf{p}_e)]$ is the far-field amplitude for the emitter dipole in vacuum. As the radiated power is proportional to the squared magnitude of the far-field amplitude, we can rewrite the factor $|\mathbf{f}|^2/|\mathbf{f}_0|^2$, for $\theta = 0°$ and $\theta = 180°$, as

$$\frac{|\mathbf{f}|^2}{|\mathbf{f}_0|^2} = \frac{4}{3}\frac{P(\theta)}{P_0},$$

where $P(\theta)$ is the half-integrated power radiated in the direction θ, which is plotted in Figure 3. Combining these expressions, we obtain (2). It is worth noting that Lorentz reciprocity [60] implies that $4P(\theta)/(3P_0)$ is equal to $\mathrm{FE}(\theta)$ for $\theta = 0°$ and 180°. This means that, for these angles, we can write the nETR as $\mathrm{nETR} \approx 16P^2(\theta)/(9P_0^2)$ and therefore use (1) to obtain an analytical result within the dipolar approximation.

References

[1] Maier SA. Plasmonics: fundamentals and applications. New York: Springer, 2007.

[2] Bharadwaj P, Deutsch B, Novotny L. Optical antennas. Adv Opt Photon 2009;1:438–83.

[3] Novotny L, van Hulst N. Antennas for light. Nat Photon 2011;5:83–90.

[4] Curto AG, Volpe G, Taminiau TH, Kreuzer MP, Quidant R, van Hulst NF. Unidirectional emission of a quantum dot coupled to a nanoantenna. Science 2010;329:930–3.

[5] Giannini V, Fernández-Domínguez AI, Heck SC, Maier SA. Plasmonic nanoantennas: fundamentals and their use in controlling the radiative properties of nanoemitters. Chem Rev 2011;111:3888–912.

[6] Agio M, Alú A. Optical antennas. Cambridge: Cambridge University Press, 2013.

[7] Tang L, Kocabas SE, Latif S, et al. Nanometre-scale germanium photodetector enhanced by a near-infrared dipole antenna. Nat Photon 2008;2:226.

[8] Knight MW, Sobhani H, Nordlander P, Halas NJ. Photodetection with active optical antennas. Science 2011;332:702–4.

[9] Chalabi H, Schoen D, Brongersma ML. Hot-electron photodetection with a plasmonic nanostripe antenna. Nano Lett 2014;14:1374–80.

[10] Cubukcu E, Kort EA, Crozier KB, Capasso F. Plasmonic laser antenna. Appl Phys Lett 2006;89:093120.

[11] Vaskin A, Kolkowski R, Koenderink FA, Staude I. Light-emitting metasurfaces. Nanophotonics 2019;8:1151.

[12] Catchpole KR, Polman A. Plasmonic solar cells. Opt Express 2008;16:21793–800.

[13] Di Vece M, Kuang Y, van Duren SNF, Charry JM, van Dijk L, Schropp REI. Plasmonic nano-antenna a-Si:H solar cell. Opt Express 2012;20:27327–36.

[14] Zhang W, Huang L, Santschi C, Martin OJF. Trapping and sensing 10 nm metal nanoparticles using plasmonic dipole antennas. Nano Lett 2010;10:1006–11.

[15] Liu N, Tang ML, Hentschel M, Giessen H, Alivisatos AP. Nanoantenna-enhanced gas sensing in a single tailored nanofocus. Nat Mater 2011;10:631–6.

[16] Reed JC, Zhu H, Zhu AY, Li C, Cubukcu E. Graphene-enabled silver nanoantenna sensors. Nano Lett 2012;12:4090–4.

[17] Xin H, Namgung B, Lee LP. Nanoplasmonic optical antennas for life sciences and medicine. Nat Rev Mater 2018;3:228–43.

[18] Hatab NA, Hsueh C-H, Gaddis AL, et al. Free-standing optical gold bowtie nanoantenna with variable gap size for enhanced Raman spectroscopy. Nano Lett 2010;10:4952–5.

[19] Huck C, Neubrech F, Vogt J, et al. Surface-enhanced infrared spectroscopy using nanometer-sized gaps. ACS Nano 2014;8:4908–14.

[20] Noginov MA, Podolskiy VA, Zhu G, et al. Compensation of loss in propagating surface plasmon polariton by gain in adjacent dielectric medium. Opt Express 2008;16:1385–92.

[21] Boriskina SV, Cooper TA, Zeng L, et al. Losses in plasmonics: from mitigating energy dissipation to embracing loss-enabled functionalities. Adv Opt Photon 2017;9:775–827.

[22] Meng L, Zhao D, Yang Y, et al. Gain-assisted plasmon resonance narrowing and its application in sensing. Phys Rev Appl 2019;11:044030.

[23] Miri M-A, Duggan RS, Alú A. Parity-time symmetry and its applications. In: Parity-time symmetry in scattering problems. Singapore: Springer Singapore, 2018:53–74.

[24] Benisty H, Degiron A, Lupu A, et al. Implementation of PT symmetric devices using plasmonics: principle and applications. Opt Express 2011;19:18004–19.

[25] Barton D, Lawrence M, Alaeian H, Baum B, Dionne J. Parity-time symmetric plasmonics. In: Parity-time symmetry and its applications. Singapore: Springer Singapore, 2018:301–49.

[26] Sounas DL, Fleury R, Alú A. Unidirectional cloaking based on metasurfaces with balanced loss and gain. Phys Rev Appl 2015;4:014005.

[27] Lupu A, Benisty H, Degiron A. Switching using PT symmetry in plasmonic systems: positive role of the losses. Opt Express 2013;21:21651–68.

[28] Wang W, Wang L-Q, Xue R-D, et al. Unidirectional excitation of radiative-loss-free surface plasmon polaritons in $\mathcal{PT}$-symmetric systems. Phys Rev Lett 2017;119:077401.

[29] Aleian H, Baum B, Jankovic V, Lawrence M, Dionne JA. Towards nanoscale multiplexing with parity-time symmetric plasmonic coaxial waveguides. Phys Rev B 2016;93:205439.

[30] Alaeian H, Dionne JA. Non-Hermitian nanophotonic and plasmonic waveguides. Phys Rev B 2014;89:075136.
[31] Alaeian H, Dionne JA. Parity-time-symmetric plasmonic metamaterials. Phys Rev A 2014;89:033829.
[32] Keshmarzi EK, Tait RN, Berini P. Spatially nonreciprocal Bragg gratings based on surface plasmons. Appl Phys Lett 2014;105:191110.
[33] Alaeian H, Dionne JA. Controlling electric, magnetic, and chiral dipolar emission with PT-symmetric potentials. Phys Rev B 2015;91:245108.
[34] Wang J, Dong HY, Shi QY, Wang W, Fung KH. Coalescence of nonreciprocal exceptional points in magnetized $\mathcal{PT}$-symmetric systems. Phys Rev B 2018;97:014428.
[35] Barton DR, Alaeian H, Lawrence M, Dionne J. Broadband and wide-angle nonreciprocity with a non-Hermitian metamaterial. Phys Rev B 2018;97:045432.
[36] Baum B, Alaeian H, Dionne JA. A parity-time symmetric coherent plasmonic absorber-amplifier. J Appl Phys 2015;117:063106.
[37] Mattheakis M, Oikonomou T, Molina MI, Tsironis GP. Phase transition in $\mathcal{PT}$ symmetric active plasmonic systems. IEEE J Sel Topics Quantum Electron 2016;22:1–6.
[38] Li Y, Argyropoulos C. PT-symmetric epsilon-near-zero plasmonic waveguides. In: 2017 IEEE International Symposium on Antennas and Propagation USNC/URSI National Radio Science Meeting 2017:691–2.
[39] Jin W, Khandekar C, Pick A, Polimeridis AG, Rodriguez AW. Amplified and directional spontaneous emission from arbitrary composite bodies: a self-consistent treatment of purcell effect below threshold. Phys Rev B 2016;93:125415.
[40] Zhang W, Wu T, Zhang X. Tailoring eigenmodes at spectral singularities in graphene-based PT systems. Sci Rep 2017;7:11407.
[41] Manjavacas A. Anisotropic optical response of nanostructures with balanced gain and loss. ACS Photonics 2016;3:1301–7.
[42] Miri M-A, Eftekhar MA, Facao M, et al. Scattering properties of PT-symmetric objects. J Opt 2016;18:075104.
[43] Duggan R, Miri M-A, Alú A. Scattering properties of parity-time symmetric nanoparticle dimers. In: 2017 IEEE International Symposium on Antennas and Propagation USNC/URSI National Radio Science Meeting, 2017:1067–8.
[44] Safari M, Albooyeh M, Simovski CR, Tretyakov SA. Shadow-free multimers as extreme-performance meta-atoms. Phys Rev B 2018;97:085412.
[45] Krasnok A, Baranov D, Li H, Miri M-A, Monticone F, Alú A. Anomalies in light scattering. 2019. arXiv:1907.06506.
[46] Alaee R, Christensen J, Kadic M. Optical pulling and pushing forces in bilayer $\mathcal{PT}$-symmetric structures. Phys Rev Appl 2018;9:014007.
[47] Miri M-A, Cotrufo M, Alú A. Anomalous optical forces in PT-symmetric waveguides. Opt Lett 2019;44:3558–61.
[48] Sakhdari M, Farhat M, Chen P-Y. $\mathcal{PT}$-symmetric metasurfaces: wave manipulation and sensing using singular points. New J Phys 2017;19:065002.
[49] Baum B, Lawrence M, Barton D, Dionne J, Alaeian H. Active polarization control with a parity-time-symmetric plasmonic resonator. Phys Rev B 2018;98:165418.
[50] Khandekar C, Jin W, Miller OD, Pick A, Rodriguez AW. Giant frequency-selective near-field energy transfer in active–passive structures. Phys Rev B 2016;94:115402.
[51] Kim J, Naik GV, Emani NK, Guler U, Boltasseva A. Plasmonic resonances in nanostructured transparent conducting oxide films. IEEE J Sel Topics Quantum Electron 2013;19:4601907.
[52] Scheel S, Szameit A. $\mathcal{PT}$-symmetric photonic quantum systems with gain and loss do not exist. Europhys Lett 2018;122:34001.
[53] Campione S, Albani M, Capolino F. Complex modes and near-zero permittivity in 3d arrays of plasmonic nanoshells: loss compensation using gain. Opt Mater Express 2011;1:1077–89.
[54] Fietz C, Soukoulis CM. Finite element simulation of microphotonic lasing system. Opt Express 2012;20:11548–60.
[55] Kolkowski R, Koenderink AF. Lattice resonances in optical metasurfaces with gain and loss. Proc IEEE 2019:1–24.
[56] Li J, Salandrino A, Engheta N. Shaping light beams in the nanometer scale: a yagi-uda nanoantenna in the optical domain. Phys Rev B 2007;76:245403.
[57] Guo A, Salamo GJ, Duchesne D, et al. Observation of $\mathcal{PT}$-symmetry breaking in complex optical potentials. Phys Rev Lett 2009;103:093902.
[58] El-Ganainy R, Makris KG, Khajavikhan M, Musslimani ZH, Rotter S, Christodoulides DN. Non-Hermitian physics and PT symmetry. Nat Phys 2018;14:11–9.
[59] Miri M-A, Alú A. Exceptional points in optics and photonics. Science 2019;363:eaar7709.
[60] Jackson JD. Classical electrodynamics. New York: Wiley, 1975.
[61] Novotny L, Hecht B. Principles of nano-optics. New York: Cambridge University Press, 2006.
[62] Martín-Cano D, Martín-Moreno L, García-Vidal FJ, Moreno E. Resonance energy transfer and superradiance mediated by plasmonic nanowaveguides. Nano Lett 2010;10:3129–34.
[63] García de Abajo FJ. Multiple scattering of radiation in clusters of dielectrics. Phys Rev B 1999;60:6086–102.